TOPOLOGICAL MATTER

Nearly quantized conductance plateau of vortex zero mode in an iron-based superconductor

Shiyu Zhu[1,2]*, Lingyuan Kong[1,2]*, Lu Cao[1,2]*, Hui Chen[1,2]*, Michał Papaj[3], Shixuan Du[1,2,4,5], Yuqing Xing[1,2], Wenyao Liu[1,2], Dongfei Wang[1,2], Chengmin Shen[1,4], Fazhi Yang[1,2], John Schneeloch[6], Ruidan Zhong[6], Genda Gu[6], Liang Fu[3], Yu-Yang Zhang[2,1,4]†, Hong Ding[1,2,4,5]†, Hong-Jun Gao[1,2,4,5]†

Majorana zero modes (MZMs) are spatially localized, zero-energy fractional quasiparticles with non-Abelian braiding statistics that hold promise for topological quantum computing. Owing to the particle-antiparticle equivalence, MZMs exhibit quantized conductance at low temperature. By using variable-tunnel–coupled scanning tunneling spectroscopy, we studied tunneling conductance of vortex bound states on $FeTe_{0.55}Se_{0.45}$ superconductors. We report observations of conductance plateaus as a function of tunnel coupling for zero-energy vortex bound states with values close to or even reaching the $2e^2/h$ quantum conductance (where e is the electron charge and h is Planck's constant). By contrast, no plateaus were observed on either finite energy vortex bound states or in the continuum of electronic states outside the superconducting gap. This behavior of the zero-mode conductance supports the existence of MZMs in $FeTe_{0.55}Se_{0.45}$.

Majorana zero modes (MZMs) obey non-Abelian statistics and have potential applications in topological quantum computation (*1*, *2*). In the past two decades, MZMs have been predicted in p-wave superconductors (*3*, *4*) and spin-orbit–coupled materials proximitized by s-wave superconductors (*5*–*8*). Experimental evidence for MZMs has been observed in various systems, including semiconductor-superconductor nanowires (*9*, *10*), topological insulator-superconductor heterostructures (*11*), and atomic chains on superconducting substrate (*12*, *13*). Recently, fully gapped bulk iron–based superconductors have emerged as a single-material platform for MZMs (*14*, *15*). Evidence for MZMs in topological vortices on the surface of $FeTe_{0.55}Se_{0.45}$ has been found with scanning tunneling microscopy/spectroscopy (STM/S) (*16*–*18*).

At sufficiently low temperatures, the conductance of an MZM exhibits a quantized plateau at the value of $2e^2/h$, where e is the electron charge and h is Planck's constant (*19*, *20*). This quantized Majorana conductance results from perfect resonant Andreev reflection guaranteed by the inherent particle-hole symmetric nature of MZM (*2*). A quantized conductance plateau has been observed in an InSb–Al nanowire system, which is consistent with the existence of MZMs (*21*). However, some alternative explanations have not been ruled out; for example, the partially separated Andreev bound state (ps-ABS) can also lead to a quantized conductance plateau that is topologically trivial (*22*–*24*). Iron-based superconductors, in which STM/S experiments observed zero-bias conductance peaks (ZBCPs) (*16*–*18*, *25*), have large topological gaps [estimated at ~0.7 meV for Fe(Te,Se) in (*16*)] and offer the possibility of observing Majorana quantized conductance without contamination from low-lying Caroli–de Gennes–Matricon bound states (CBSs) (*16*, *18*). Results suggesting quantized conductance have been reported for $(Li_{0.84}Fe_{0.16})OHFeSe$ (*26*).

Motivated by the above prospects, we used a variable-tunnel–coupling STM/S method to study the Majorana conductance over a large range of tip-sample distance in vortex cores of $FeTe_{0.55}Se_{0.45}$ (Fig. 1A). The effective electron temperature (T_{eff}) of our STM is 377 mK, as calibrated by tunneling into aluminum (fig. S1). In STM/S, the tunnel coupling can be continuously tuned by changing the tip-sample distance (d), which correlates with the tunnel-barrier conductance ($G_N \equiv I_t/V_s$, where I_t is the tunneling current and V_s is the setpoint voltage) (*16*). With a 2-T magnetic field applied perpendicular to the sample surface, we observed a sharp ZBCP at a vortex core (Fig. 1B). This ZBCP neither disperses nor splits across the vortex core, as expected for an isolated MZM in a quantum-limited vortex (*16*–*18*, *25*). We performed tunnel-coupling–dependent measurement on the observed ZBCP. By putting the STM tip at the center of a topological vortex (*18*), we recorded a set of differential conductance (dI/dV) spectra with different tip-sample distances (Fig. 1C). The ZBCP remained a well-defined peak located at zero energy [voltage offset calibration under different tunnel couplings is discussed in (*27*)]. We observed a distinct behavior of ZBCP under different G_N (Fig. 1C): The ZBCP peak height saturates at a relatively high tunnel coupling (Fig. 1F), whereas the high-bias conductance outside the superconducting gap increases monotonically as a function of G_N. This behavior can be better visualized in a three-dimensional plot (Fig. 1D) and a color-scale plot (Fig. 1E) that introduce an additional axis for G_N. The zero-bias conductance reaches a plateau when G_N is around $0.3\ G_0$ ($G_0 \equiv 2e^2/h$). Two plots of conductance curves as a function of G_N were extracted from Fig. 1, C to E. The zero-bias conductance barely changes over a wide range of G_N ($0.3\ G_0$ ~ $0.9\ G_0$); the average plateau conductance (G_P) is equal to $0.64\ G_0$ (Fig. 1F). By contrast, the high-bias conductance at ±1.5 and −4.5 meV (Fig. 1G) changes by a factor of more than three as the tip-sample distance varies.

To examine the particle-hole-symmetric nature of the MZMs, we compared and contrasted conductance behavior of zero-energy MZMs and finite-energy CBSs. As demonstrated previously, there are two distinct types of vortices: topological vortices with MZM and ordinary vortices without MZM, differing by a half-integer level shift of vortex bound states (*18*). First, we performed a tunnel-coupling–dependent measurement on a topological vortex (Fig. 2, A and B), which showed an MZM and the first CBS level located at 0 and ± 0.31 meV, respectively. In contrast to MZM, we found that the conductance of finite-energy CBS keeps increasing with G_N and shows no plateau. We also carried out measurements on an ordinary vortex. A dI/dV spectrum showed a CBS with half-odd-integer quantization (Fig. 2C), in which the first three levels of CBSs were located at ±0.13, ±0.39, and ±0.65 meV, respectively. Again, the conductance values of all the CBSs kept increasing and had no plateau feature in the tunnel-coupling–dependent measurement (Fig. 2D). As another check, we repeated the measurement for the same location at zero magnetic field (Fig. 2, E and F) and observed a hard superconducting gap. The zero-bias conductance and the high-bias conductance were plotted as functions of G_N (Fig. 2F, middle and bottom, respectively). It is evident that both curves keep increasing as the tunnel coupling increases. This observation can be confirmed in a z-offset plot, with a larger z-offset corresponding to a smaller tip-sample distance (fig. S3). Therefore, the conductance plateau feature has only been observed in ZBCP, which indicates behavior specific to Majorana modes.

The plateau behavior of the zero-bias conductance provides evidence for the Majorana-induced resonant Andreev reflection (*19*, *20*). It has been well understood that a perfect transmission of electrons can occur in a symmetric double-barrier system by means of

[1]Beijing National Laboratory for Condensed Matter Physics and Institute of Physics, Chinese Academy of Sciences, Beijing 100190, China. [2]School of Physical Sciences, University of Chinese Academy of Sciences, Beijing 100190, China. [3]Department of Physics, Massachusetts Institute of Technology, Cambridge, MA 02139, USA. [4]CAS Center for Excellence in Topological Quantum Computation, University of Chinese Academy of Sciences, Beijing 100190, China. [5]Songshan Lake Materials Laboratory, Dongguan, Guangdong 523808, China. [6]Condensed Matter Physics and Materials Science Department, Brookhaven National Laboratory, Upton, NY 11973, USA.
*These authors contributed equally to this work.
†Corresponding author. Email: hjgao@iphy.ac.cn (H.-J.G.); dingh@iphy.ac.cn (H.D.); zhangyuyang@ucas.ac.cn (Y.-Y.Z.)

Downloaded from http://science.sciencemag.org/ on January 9, 2020

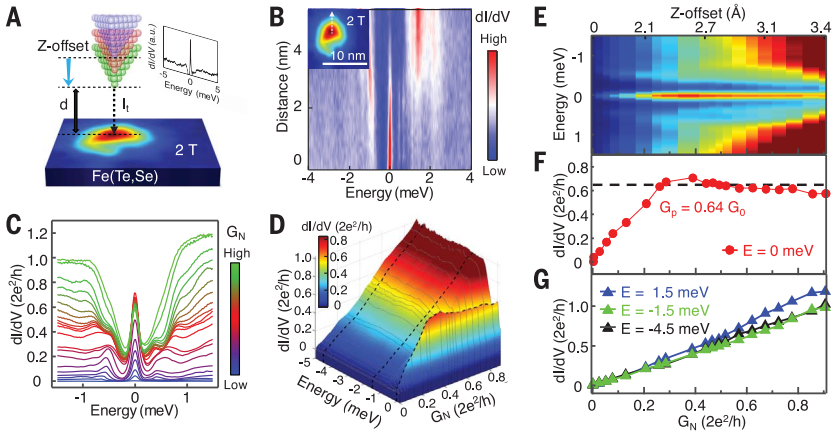

Fig. 1. Zero-bias conductance plateau observed on $FeTe_{0.55}Se_{0.45}$. (**A**) A schematic of variable-tunnel–coupling STM/S method. A zero-bias conductance map under 2.0 T is shown on a sample surface. A *dI/dV* spectrum measured at the center of the vortex core (V_s = −5 mV, I_t = 500 pA, V_{mod} = 0.02 mV) is shown in the top right inset; a sharp ZBCP is observed. When the tunneling current (I_t) is adjusted by the STM regulation loop, the tunnel coupling between the STM tip and the MZM can be tuned continuously with the tip-sample distance (*d*). Larger tunnel coupling corresponds to smaller *d* and larger tunneling-barrier conductance ($G_N = I_t/V_s$, where V_s is the setpoint voltage). *z*-offset can be read out simultaneously, which indicates the absolute *z* direction motion of the STM tip. (**B**) A line-cut intensity plot along the dashed white arrow in the inset, measured from the same vortex shown in (A), showing a stable MZM across the vortex core. (**C**) An overlapping plot of *dI/dV* spectra under different tunnel coupling values parameterized in G_N. The blue curve is measured under the smallest G_N, whereas the green curve is measured with the largest G_N. (**D**) A three-dimensional plot of tunnel coupling–dependent measurement, $dI/dV(E, G_N)$. For clarity, only the data points in the energy range of [−5.0, 0.2] meV are shown. (**E**) A color-scale plot of (C) within the energy range of [−1.5, 1.5] meV that shows the spectra as a function of G_N. The *z*-offset information, which was taken simultaneously by STM, is provided on the top axis. The maximum distance the tip approached is 3.4 Å. This plot shares the same color bar with (D). (**F**) A horizontal line-cut at the zero-bias from (E). The conductance curve shows a plateau behavior with the plateau conductance (G_P) equal to (0.64 ± 0.04) G_0. (**G**) Horizontal line-cuts at high-bias values from (E). The absence of a conductance plateau on these curves indicates conventional tunneling behavior at the energy of continuous states. All the data were measured at T_{eff} = 377 mK.

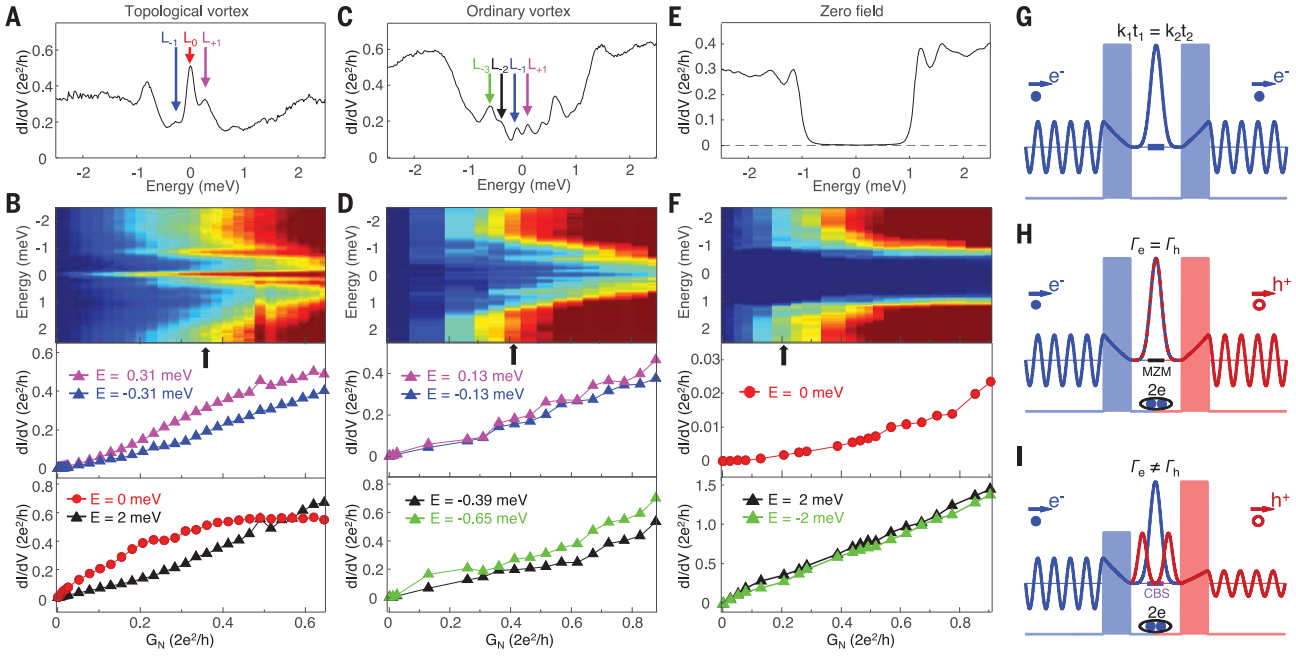

Fig. 2. Majorana-induced resonant Andreev reflection. (**A**) A *dI/dV* spectrum measured at the center of a topological vortex (V_s = −5 mV, I_t = 140 nA, V_{mod} = 0.02 mV), which shows a MZM (red arrow) coexisting with CBSs located at ±0.31 meV (indicated with magenta and blue arrows). (**B**) A tunnel-coupling–dependent measurement on the vortex shown in (A) at 2 T. (Top) A color-scale plot, $dI/dV(E, G_N)$. The G_N position of (A) is indicated with a black arrow. (Middle) Tunnel coupling evolution of CBS conductance, which shows no plateau behavior. (Bottom) Tunnel coupling evolution of conductance at the energies of 0 meV (red circles, exhibiting a plateau) and 2 meV (black triangles, monotonically increasing). (**C**) A *dI/dV* spectrum measured at the center of an ordinary vortex (V_s = −5 mV, I_t = 160 nA, V_{mod} = 0.02 mV), which clearly shows three levels of CBS at ±0.13 meV (magenta and blue arrows), ±0.39 meV (black arrow), and ±0.65 meV (green arrow). (**D**) Similar to (B), but measured on the vortex shown in (C). (Middle and bottom) Tunnel coupling evolution of CBS conductance, showing no plateau feature. (**E**) A *dI/dV* spectrum measured at 0 T (V_s = −5 mV, I_t = 80 nA, V_{mod} = 0.02 mV). A hard superconducting gap can be seen. (**F**) Similar to (B) and (D), but measured under 0 T. (Middle) Tunnel-coupling evolution of zero-bias conductance (normal metal-superconductor junction case). (Bottom) Tunnel coupling evolution of conductance at the above gap energy (normal metal–normal metal junction case). There is no plateau behavior at 0 T. (**G**) A schematic of resonant tunneling through a symmetric double-barrier system. The wave function evolution of a tunneled electron is shown. *kt* is penetration constant. (**H**) The double-barrier view of the MZM-induced resonant Andreev reflection. The blue and red colors indicate the electron and hole process, respectively. The equivalence of particle and hole components in MZM ensures the same tunnel coupling on electron and hole barrier ($\Gamma_e = \Gamma_h$). (**I**) The double-barrier view of Andreev reflection mediated by a CBS. The arbitrary mixing of particle-hole components in CBS breaks the resonance condition. All the data were measured at T_{eff} = 377 mK.

Downloaded from http://science.sciencemag.org/ on January 9, 2020

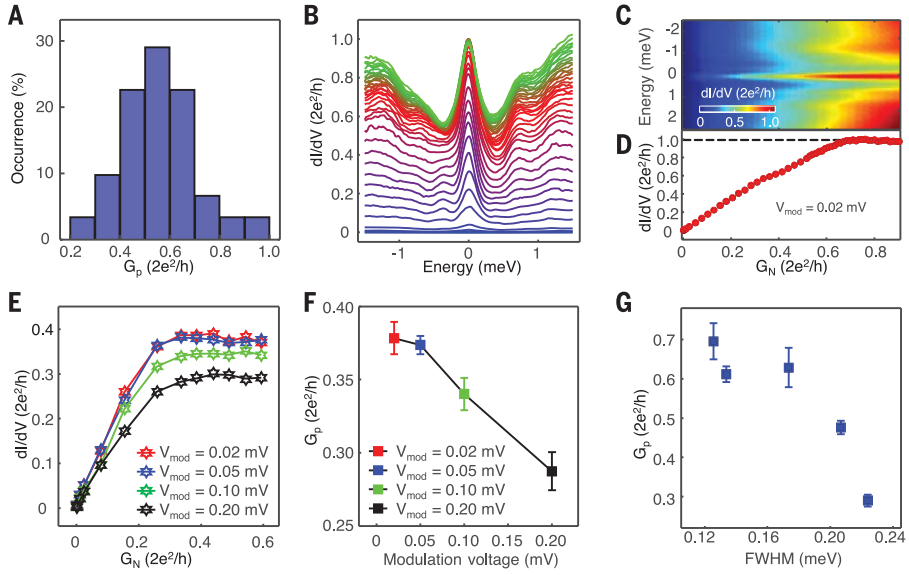

Fig. 3. The conductance variation of Majorana plateau. (**A**) A histogram of the G_P from 31 sets of data, which were measured with the same instrument. Sorting of the plateau conductance (G_P) in the order of increasing magnitude can be found in fig. S9 (V_s = −5 mV, V_{mod} = 0.02 mV). (**B**) The overlapping plot of 38 *dI/dV* spectra selected from a topological vortex that reaches a quantized conductance plateau (V_s = −5 mV, V_{mod} = 0.02 mV). (**C**) A color-scale plot of (B) within the energy range of [−2.5, 2.5] meV that shows the spectra as a function of G_N. (**D**) A horizontal line-cut at the zero-bias from (C). The conductance curve shows that the conductance plateau reaches G_0. (**E**) A series of tunnel-coupling–dependent measurements on the same MZM, with four modulation voltages of 0.02, 0.05, 0.10, and 0.20 mV. (**F**) The plot of G_P as a function of modulation voltage of the data shown in (E). (**G**) Relationship between FWHM of ZBCP and G_P, obtained from five different MZMs measured at the same experimental conditions, suggesting that the quasiparticle poisoning effect affects the plateau value. The FWHM were extracted from the spectrum measured at a large tip-sample distance with the same experimental parameters (V_s = −5 mV, I_t = 500 pA, V_{mod} = 0.02 mV). All the data were measured at T_{eff} = 377 mK.

resonant tunneling through a single quasistationary bound state (Fig. 2G). The transmission on resonance is e^2/h independent of tunnel coupling, as long as it is identical for the two barriers (*28*, *29*). In the case of electron tunneling from a normal electrode through a barrier into a superconductor, the Andreev reflection process (*30*) converts the incident electron into an outgoing hole in the same electrode, resulting in a double-barrier system in the particle-hole Hilbert space. Moreover, in the case of Andreev reflection by means of a single MZM, the equal amplitude of particle-hole components, caused by the particle-antiparticle equivalence of MZM, ensures an identical tunnel coupling with electron and hole in the same electrode ($\Gamma_e = \Gamma_h$) (Fig. 2H). Thus, the resonant Andreev reflection mediated by an MZM leads to a $2e^2/h$–quantized zero-bias conductance plateau, independent of the strength of tunnel coupling at zero temperature (*19*, *20*, *31*, *32*). By contrast, low-energy CBSs (*33*, *34*) and other trivial subgap states (*22*) do not have the Majorana symmetry, resulting in unequal weights for electron-hole components. The relationship of $\Gamma_e = \Gamma_h$ is broken in a CBS-mediated Andreev reflection (Fig. 2I), which leads to an absence of a conductance plateau (Fig. 2B, middle). Moreover, the observed zero-bias conductance plateau in the vortex core disappears after the magnetic field is removed (Fig. 3, E and F) and hence cannot be attributed to quantum ballistic transport (*35*–*40*).

We observed the plateau behavior of ZBCPs repeatedly in many topological vortices [31 plateau features out of 60 measurements (*41*)]. We performed a statistical analysis of the observed plateau values G_P and found that most values of G_P are located around 40 to 70% of $G_0 = 2e^2/h$ (Fig. 3A). In one case, the plateau conductance reaches G_0 (Fig. 3, B to D). Both instrumental broadening and quasiparticle poisoning in our system can potentially induce deviation of G_P from the theoretical quantized value $2e^2/h$. To examine the possible effect of instrumental broadening on Majorana conductance plateau, we deliberately increased the instrumental broadening by varying the modulation voltage (V_{mod}), which is defined by the zero-to-peak amplitude of lock-in excitation. This allowed us to study the V_{mod}-evolution of the Majorana conductance plateau on a given topological vortex (Fig. 3, E and F). We found that larger V_{mod} leads to stronger suppression of G_P of MZM. In addition, we noticed that the values of conductance plateaus are correlated with the full width of half maximum (FWHM) of the ZBCP measured under a large tip-sample distance limit. We found that G_P decreases with increasing FWHM (Fig. 3G) (detailed data are shown in fig. S5). This indicates that the quasiparticle poisoning effect (*42*, *43*) might also play a role in reducing the conductance plateau value; the poisoning rate is expected to be spatially nonuniform in $FeTe_{0.55}Se_{0.45}$, which has intrinsic inhomogeneities.

We also checked the reversibility of the process of varying tunneling coupling in STM and found that both the topography and the conductance plateau can be reproduced during two repeated sequences of varying tunneling coupling (fig. S8), indicating the absence of irreversible damage of the tip and the sample during measurements. Other mechanisms related to zero-bias conductance plateau, such as inhomogeneity-induced ps-ABS (*22*–*24*) and class-D weak antilocalization (*44*), cannot be definitively excluded; complete understanding of our experiments requires further theoretical efforts. Our observation of a zero-bias conductance plateau in the two-dimensional vortex case, which approaches the quantized conductance of $2e^2/h$, provides spatially resolved spectroscopic evidence for Majorana-induced resonant electron transmission into a bulk superconductor, moving one step further toward the braiding operation applicable to topological quantum computation.

REFERENCES AND NOTES

1. A. Y. Kitaev, *Ann. Phys.* **303**, 2–30 (2003).
2. C. Nayak, S. H. Simon, A. Stern, M. Freedman, S. Das Sarma, *Rev. Mod. Phys.* **80**, 1083–1159 (2008).
3. A. Y. Kitaev, *Phys. Uspekhi* **44** (10S), 131–136 (2001).
4. N. Read, D. Green, *Phys. Rev. B Condens. Matter Mater. Phys.* **61**, 10267–10297 (2000).
5. L. Fu, C. L. Kane, *Phys. Rev. Lett.* **100**, 096407 (2008).
6. J. D. Sau, R. M. Lutchyn, S. Tewari, S. Das Sarma, *Phys. Rev. Lett.* **104**, 040502 (2010).
7. R. M. Lutchyn, J. D. Sau, S. Das Sarma, *Phys. Rev. Lett.* **105**, 077001 (2010).
8. Y. Oreg, G. Refael, F. von Oppen, *Phys. Rev. Lett.* **105**, 177002 (2010).
9. V. Mourik *et al.*, *Science* **336**, 1003–1007 (2012).
10. R. M. Lutchyn *et al.*, *Nat. Rev. Mater.* **3**, 52–68 (2018).
11. H. H. Sun *et al.*, *Phys. Rev. Lett.* **116**, 257003 (2016).
12. S. Nadj-Perge, I. K. Drozdov, B. A. Bernevig, A. Yazdani, *Phys. Rev. B Condens. Matter Mater. Phys.* **88**, 020407 (2013).
13. S. Nadj-Perge *et al.*, *Science* **346**, 602–607 (2014).
14. Z. Wang *et al.*, *Phys. Rev. B Condens. Matter Mater. Phys.* **92**, 115119 (2015).
15. P. Zhang *et al.*, *Science* **360**, 182–186 (2018).
16. D. Wang *et al.*, *Science* **362**, 333–335 (2018).
17. T. Machida *et al.*, *Nat. Mater.* **18**, 811–815 (2019).
18. L. Kong *et al.*, *Nat. Phys.* **15**, 1181–1187 (2019).
19. K. T. Law, P. A. Lee, T. K. Ng, *Phys. Rev. Lett.* **103**, 237001 (2009).
20. M. Wimmer, A. R. Akhmerov, J. P. Dahlhaus, C. W. J. Beenakker, *New J. Phys.* **13**, 053016 (2011).
21. H. Zhang *et al.*, *Nature* **556**, 74–79 (2018).
22. C. X. Liu, J. D. Sau, T. D. Stanescu, S. Das Sarma, *Phys. Rev. B* **96**, 075161 (2017).
23. C. Moore, T. D. Stanescu, S. Tewari, *Phys. Rev. B* **97**, 165302 (2018).
24. C. Moore, C. C. Zeng, T. D. Stanescu, S. Tewari, *Phys. Rev. B* **98**, 155314 (2018).
25. Q. Liu *et al.*, *Phys. Rev. X* **8**, 041056 (2018).
26. C. Chen *et al.*, *Chin. Phys. Lett.* **36**, 057403 (2019).
27. Materials and methods are available as supplementary materials.

Downloaded from http://science.sciencemag.org/ on January 9, 2020

28. R. Tsu, L. Esaki, *Appl. Phys. Lett.* **22**, 562–564 (1973).
29. L. L. Chang, L. Esaki, R. Tsu, *Appl. Phys. Lett.* **24**, 593–595 (1974).
30. G. E. Blonder, M. Tinkham, T. M. Klapwijk, *Phys. Rev. B Condens. Matter* **25**, 4515–4532 (1982).
31. K. Flensberg, *Phys. Rev. B Condens. Matter Mater. Phys.* **82**, 180516 (2010).
32. F. Setiawan, C. X. Liu, J. D. Sau, S. Das Sarma, *Phys. Rev. B* **96**, 184520 (2017).
33. C. Caroli, P. G. De Gennes, J. Matricon, *Phys. Lett.* **9**, 307–309 (1964).
34. H. F. Hess, R. B. Robinson, J. V. Waszczak, *Phys. Rev. Lett.* **64**, 2711–2714 (1990).
35. C. W. Beenakker, J. G. Williamson, L. P. Kouwenhoven, C. T. Foxon, *Phys. Rev. Lett.* **60**, 848–850 (1988).
36. J. Kammhuber *et al*., *Nano Lett.* **16**, 3482–3486 (2016).
37. C. W. Beenakker, *Phys. Rev. B Condens. Matter* **46**, 12841–12844 (1992).
38. M. Kjaergaard *et al*., *Nat. Commun.* **7**, 12841 (2016).
39. H. Zhang *et al*., *Nat. Commun.* **8**, 16025 (2017).
40. Ö. Gül *et al*., *Nat. Nanotechnol.* **13**, 192–197 (2018).
41. That we did not observe a plateau feature in the other 29 cases is because of the instability of the vortices during the tip-approaching process [(*27*), section 5].
42. J. R. Colbert, P. A. Lee, *Phys. Rev. B Condens. Matter Mater. Phys.* **89**, 140505 (2014).
43. I. Martin, D. Mozyrsky, *Phys. Rev. B Condens. Matter Mater. Phys.* **90**, 100508 (2014).
44. H. Pan, W. S. Cole, D. Jay, Sau and S. Das Sarma, Generic quantized zero-bias conductance peaks in superconductor-semiconductor hybrid structures. arXiv:1906.08193 [cond-mat.mes-hall] (2019).
45. S. Zhu *et al*., Nearly quantized conductance plateau of vortex zero mode in an iron-based superconductor. Zenodo (2019); doi:10.5281/zenodo.3514211

ACKNOWLEDGMENTS

We thank P. A. Lee, C.-X. Liu, and G. Su for helpful discussions and A.-W. Wang, J.-H. Yan, and Q. Huan for technical assistance. **Funding:** The work at IOP is supported by grants from the Ministry of Science and Technology of China (2019YFA0308500, 2015CB921000, 2015CB921300, and 2016YFA0202300), the National Natural Science Foundation of China (61888102 and 11888101), and the Chinese Academy of Sciences (XDB28000000, XDB30000000, and 112111KYSB20160061). L.F. and G.G. are supported by the U.S. Department of Energy (DOE) (DE-SC0019275 and DE-SC0012704, respectively). J.S. and R.Z. are supported by the Center for Emergent Superconductivity, an Energy Frontier Research Center funded by the DOE. **Author contributions:** H.-J. G. and H.D. designed STM experiments. S.Z., L.C., H.C., Y.X., and Y-Y.Z. performed STM experiments with assistance of W.L., F.Y., and C.S.; J.S., R.Z., and G.G. provided samples. L.F. provided theoretical explanations. Y.-Y.Z., S.D., S.Z., and L.K. processed experimental data and wrote the manuscript. All the authors participated in analyzing experimental data, plotting figures, and writing the manuscript. H.D. and H.-J.G. supervised the project. **Competing interests:** The authors declare that they have no competing interests. **Data and materials availability:** The data presented in this paper can be found in (*45*).

SUPPLEMENTARY MATERIALS

science.sciencemag.org/content/367/6474/189/suppl/DC1
Materials and Methods
Supplementary Text
Figs. S1 to S9
References (*46*–*48*)

15 February 2019; resubmitted 29 July 2019
Accepted 7 November 2019
10.1126/science.aax0274

Downloaded from http://science.sciencemag.org/ on January 9, 2020

Science

Nearly quantized conductance plateau of vortex zero mode in an iron-based superconductor

Shiyu Zhu, Lingyuan Kong, Lu Cao, Hui Chen, Michal Papaj, Shixuan Du, Yuqing Xing, Wenyao Liu, Dongfei Wang, Chengmin Shen, Fazhi Yang, John Schneeloch, Ruidan Zhong, Genda Gu, Liang Fu, Yu-Yang Zhang, Hong Ding and Hong-Jun Gao

Science **367** (6474), 189-192.
DOI: 10.1126/science.aax0274originally published online December 12, 2019

Reaching a conductance plateau

The surface of the iron-based superconductor $FeTe_{0.55}Se_{0.45}$ satisfies the necessary conditions to support topological superconductivity. Under the application of a magnetic field, vortices with zero-bias peaks that are consistent with Majorana bound states have been observed. Using scanning tunneling spectroscopy, Zhu *et al.* studied the conductance of these states as the tip-sample distance was reduced (see the Perspective by Sau). The researchers found that the value of the conductance increased and eventually saturated. For one of the vortices they studied, the conductance reached a quantized value that is characteristic of the Majorana bound states.

Science, this issue p. 189; see also p. 145

ARTICLE TOOLS http://science.sciencemag.org/content/367/6474/189

SUPPLEMENTARY MATERIALS http://science.sciencemag.org/content/suppl/2019/12/11/science.aax0274.DC1

RELATED CONTENT http://science.sciencemag.org/content/sci/367/6474/145.full

REFERENCES This article cites 48 articles, 4 of which you can access for free
http://science.sciencemag.org/content/367/6474/189#BIBL

PERMISSIONS http://www.sciencemag.org/help/reprints-and-permissions

Use of this article is subject to the Terms of Service

Science (print ISSN 0036-8075; online ISSN 1095-9203) is published by the American Association for the Advancement of Science, 1200 New York Avenue NW, Washington, DC 20005. The title *Science* is a registered trademark of AAAS.

Copyright © 2020 The Authors, some rights reserved; exclusive licensee American Association for the Advancement of Science. No claim to original U.S. Government Works

Downloaded from http://science.sciencemag.org/ on January 9, 2020